Multicoincidence Mass Spectrometry Applied to Hexamethyldisilane Excited around the Si 2p Edge

M. Simon,*[,†,‡] T. Lebrun,[†,‡,§] R. Martins,[⊥] G. G. B. de Souza,[⊥] I. Nenner,[†,‡] M. Lavollee,[†] and P. Morin[†,‡]

L.U.R.E., Bat 209d, Université Paris-Sud, 91405 Orsay, Cedex, France, C.E.A., CEN Saclay, DRECAM, SPAM, 91191 Gif sur Yvette, France, Physics Division, Argonne National Laboratory, Argonne, Illinois 60439, and Instituto de Quimica, UFRJ, Cidade Universitaria, 21910 Rio de Janeiro, Brazil

Received: November 23, 1992; In Final Form: February 23, 1993

Photoelectron–photoion–photoion coincidence (PEPIPICO) mass spectrometry is applied to Si 2p core ionization. The ion yield spectrum is compared to the spectrum of the tetramethylsilane molecule in order to point out resonances due to the Si–Si chemical bond. Simple coincidence mass spectra are dominated by the $SiC_3H_9^+$ fragment ion and do not show a strong dependence on photon wavelength. PEPIPICO spectra demonstrate that dissociation dynamics is dominated by stepwise fragmentation of $SiC_3H_9^+$ and that double ionization always involves Si–Si chemical bond rupture, shown to be faster than the Si–C rupture. We discuss the results in term of a fast decay of Si–Si into singly and doubly charged molecules followed by a cascade of slow fragmentation and isomerization of $SiC_3H_9^+$.

Introduction

In the past few years, considerable interest has been developed in the study of the dissociation processes of core excited molecules[1-6] because of possible site-selective fragmentation pathways. Our recent work on tetrahedral silicon compound molecules such as SiH_4,[7] $Si(CH_3)_4$,[8] and SiF_4[9] photoexcited near the Si 2p ionization edge shows that the nature of and the intensity ratio between single- and double-ionization decay channels vary strongly with the photon energy in the region of resonances, especially when the comparison is made below and above the core ionization limit, leading thus to different dissociation channels. For a discrete core-excited state, the excited electron in the valence electron cloud, which acts as a spectator or a nonspectator during the electronic decay channels, controls the nature of the final electronic states of the ion mostly with a single positive charge ion and its subsequent fragmentation. In contrast, in the core ionization continuum, normal Auger (including cascade Auger) processes explain the enhancement of double- (or triple-) ionization channels at the expense of single-ionization ones, giving rise to the observation of lighter fragments.

Mass spectrometry of polymethylsilanes and siloxanes has been the subject of many studies because of the very high stability of the trimethylsilyl, $Si(CH_3)_3^+$, ion.[10-12]

In the present work, we report new mass spectrometry measurements with the multicoincidence technique known as PEPIPICO mass spectrometry or charge separation mass spectrometry)[13] (CSMS) applied to hexamethyldisilane, $Si_2(CH_3)_6$ (HMDS), photoexcited near the Si 2p edge (i.e., from 100- to 130-eV photon energy). The interest of this molecule compared to the previously studied monosilane molecules is the presence of Si–Si and Si–C bonds with different strengths. The different bonding pattern of the silicon atoms in HMDS is shown to affect the resonance pattern near the Si 2p edge compared to those of tetramethylsilane[8] (Me_4Si), for which the silicon atom is bound only to carbon atoms. The main purpose of the present work is to study the dissociation dynamics of such a core-excited molecule after single, double, and triple ionization, though this technique also allows analysis of metastable states. The problem of two-, three-, and four-body fragmentation is studied by analysis of coincidence peak shapes, giving a detailed view of the cascade fragmentation processes. The influence of core ionization on the final fragmentation pattern is also examined.

Experimental Section

The apparatus has been described in detail elsewhere.[14] Briefly, the UV synchrotron radiation emitted from the SuperACO storage ring is focused on the entrance slit of a plane grating monochromator, providing a high flux (6×10^{11} photons/(Å·s) with a 100-mA ring current) in the 20–140-eV range with an energy bandwidth of 100 meV at 100 eV. The monochromatic beam is refocused at the center of the interaction chamber where it crosses at right angles an effusive gas jet. A strong electrostatic field (2000 V/cm) extracts the ions and electrons from the ionization region. The ions are swept into a second acceleration region (2500 V/cm) and then pass into a field-free 12-cm-long drift tube. The apparatus is optimized to avoid discrimination of ions with respect to their mass or kinetic energy. It allows high counting rates because of high detection efficiencies and short time of flight of the ions, which are typically in the range of 1 μs. Electrons and ions are detected by microchannel plates, supplying respectively the start and stop of a multihit time-to-digital converter (TDC). The main advantage of such a TDC is that several consecutive stops can be recorded within an adjusted time window. Time of flight of ions arising from single- and double-coincidence type are simultaneously stored, and all events are treated in real time through a MacII microcomputer. We have taken different levels of coincidence spectra:

PEPICO spectra provide conventional mass spectra, adding the sum of single and multiple dissociative ionization.

PEPIPICO spectra reflect mainly pairs of singly charged fragment ions originating from the fragmentation of the doubly charged parent molecule. As we will see in details below, the shape of the coincidence peak provides, even for three- and four-body reactions, a realistic mechanism.

HMDS is commercially available and was purchased from Janssen Chimica Co. with a purity of 97%.

Total Ion Yield

We present in Figure 1 the total ion yield spectrum of HMDS in the region of the Si 2p ionization edge (i.e., from 100- to 118-

* Author to whom correspondence should be addressed.
† Université Paris-Sud.
‡ DRECAM.
§ Argonne National Laboratory.
⊥ Cidade Universitaria.

0022-3654/93/2097-5228$04.00/0

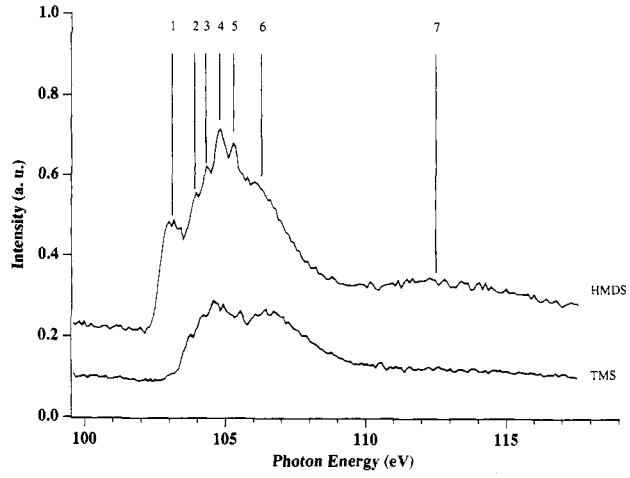

Figure 1. Total ion yield spectra of hexamethyldisilane and tetramethylsilane around the Si 2p threshold.

TABLE I: Photon Energy Position of the Different Features Measured in the Ion Yield Spectrum of HMDS around the Si 2p Threshold[a]

peak	energy (eV)	peak	energy (eV)
1	103.1	5	105.3
2	103.9	IP[15]	106.2
3	104.3	6	106.3
4	104.8	7	112.5

[a] The threshold was determined by photoelectron spectroscopy.

eV photon energy). This spectrum mimics the photoabsorption spectrum because of the very low fluorescence yield in this energy range.

We observe seven resonances labeled 1–7. The photon energies for all bands are reported in Table I.

Taking the Si $2p_{3/2}$ edge at 106.2 eV as determined by threshold electron spectroscopy,[15] we find that five structures are observed in the discrete spectrum—one sits on the ionization edge and a wide one lies in the continuum. Comparing this spectrum with the total ion yield spectrum of tetramethylsilane,[8] we readily see that resonances 2–6 are observed in the same energy range for both molecules. In contrast, resonances 1 and 7 are additional features. It is tempting at this point to associate them to the presence of the Si–Si bond, whereas all others would represent the signature of three methyl groups linked to one silicon atom. At this time, there are no calculations related to this core-excited molecule, but a correlation has been proposed by Sette et al.[16] between the energies of unoccupied orbitals and the bond length for weakly bound molecules. HMDS fits into this category since the Si–Si bond energy amounts to 265 kJ/mol.[17] According to Sette et al.,[14] one should observe a low-lying σ^* (Si–Si) antibonding orbital, and indeed resonance 1 in Figure 1 is a good candidate. This raises the question of the ordering of unoccupied orbitals in this molecule. Berkovitch-Yellin et al.[18] performed a ground-state calculation at the Hartree–Fock–Slater level introducing some Si d function in the basis set. They found four low-lying unoccupied valence orbitals $7e_{1u}$, $9a_{1g}$, $8a_{2u}$, and $9a_{2u}$. These authors claim that the lowest unoccupied orbital in energy is the $7e_{1u}$ orbital, but they also imply that the proposed ordering of the other unoccupied orbitals (mostly Si–Si or Si–C antibonding) has to be taken as qualitative because they lie very close in energy, giving the corresponding excited states a pronounced delocalized character over the molecule. In the absence of calculations on the core-excited species, we are left with the very crude assignment that resonance 1 results mainly from a monoelectronic transition into the $7e_{1u}$ antibonding Si–Si valence orbital. Notice that this core-excited state is also partly delocalized over the methyl groups. This point is of great importance in the following discussion since the search for bond-selective fragmentation is one of the motivations of the present study. Despite the fact that at least three more valence excited states are expected, Rydberg series of the *n*d and *n*s type must also be considered as for the silane molecule.[7] However, in Si 2p photoabsorption spectra of tetrahedral silicon compounds,[8,9] Rydberg core-excited states probably have a small oscillator strength when the ligand is a methyl group.[19] This is probably because the Si–C distance is too large to allow a significant Rydberg valence mixing of low-lying Rydberg states (*n*p-like), mixing which is necessary to account for a large oscillator strength. In the present case, the situation may be similar because of equivalent Si–C distances. Therefore, it is likely that the spectrum in Figure 1 can be interpreted only in terms of transition into valence states.

Shape resonance is probably responsible for the features seen in the continuum (see Figure 1), especially resonance 7, and the increase in intensity of this resonance as one moves from tetramethylsilane to HMDS may be due to the increase in the number of methyl groups. The assignment of a structure corresponding to resonance 7 is not clear. It would be interesting to know whether it is a one-electron resonance and whether it corresponds to the scattering of one Si 2p electron by the neighboring silicon atom.

One-Dimensional Spectra

PEPICO Spectra and Assignment. We present in Figure 2 PEPICO spectra of HMDS recorded at selected photon energies: below resonance 3, on resonance 3, and above the Si 2p ionization edge. These spectra correspond to the arrival of only one ion during the open time window. They therefore contain contributions of single ionization, but because the ion detection efficiency is lower than 1, they also include the contribution of dissociative multiple ionization where only one ion has been detected.

The main fragment is $SiC_3H_9^+$. It corresponds to the Si–Si bond breaking. This ion is particularly important in the mass spectrometry of methylsilanes, polymethylsilanes, and siloxanes as well as silylated compounds.[10] Its thermochemistry has been the subject of a number of studies.[10–12] The next most important ions are $SiCH_3^+$ as well as the rearranged $SiCH_5^+$. They result from the breakage of several Si–C bonds in addition to the Si–Si one. The presence of fragments like $Si_2C_xH_{3x}^+$ with $x = 4$–6 shows that some events result from the cleavage of one or more Si–C bonds while keeping the Si–Si bond intact. This latter observation is of interest since the Si–C bond is stronger than the Si–Si one. According to the work of Szepes and Baer[17] at lower energy, the rate for breaking one Si–Si bond is always greater than the rate for breaking one Si–C. These authors also found that the dissociation dynamics are fully compatible with a statistical redistribution of energy.[20] After the electronic ejection, the molecule has enough time to redistribute electronic energy into vibrational energy among all its degrees of freedom according to the various density of states before dissociation via internal conversion. We cannot perform such calculations in our case because the internal energy of the residual ion is not selected.

As can be seen in Figure 2, the fragmentation of the molecule increases as one moves from the off-resonance to the resonance region and above. This can be due to at least two factors: (1) On resonance, resonant Auger decay produces highly excited singly charged ions leading to more fragmentation. This effect has already be seen with core excitation of iron–carbonyl–nitrosyl $Fe(CO)_2(NO)_2$.[21] This has to be confirmed by deexcitation spectra measurements. (2) Above threshold, the double-ionization cross section increases because of normal Auger decay, and doubly charged ions are likely to dissociate. This leads to production of light fragments (see below). This effect has already been established in tetramethylsilane.[22]

Rearrangement Reactions. Some of the fragments shown in Figure 2 require either a multicenter concerted dissociation or isomerization previous to single-bond rupture: one bond is broken

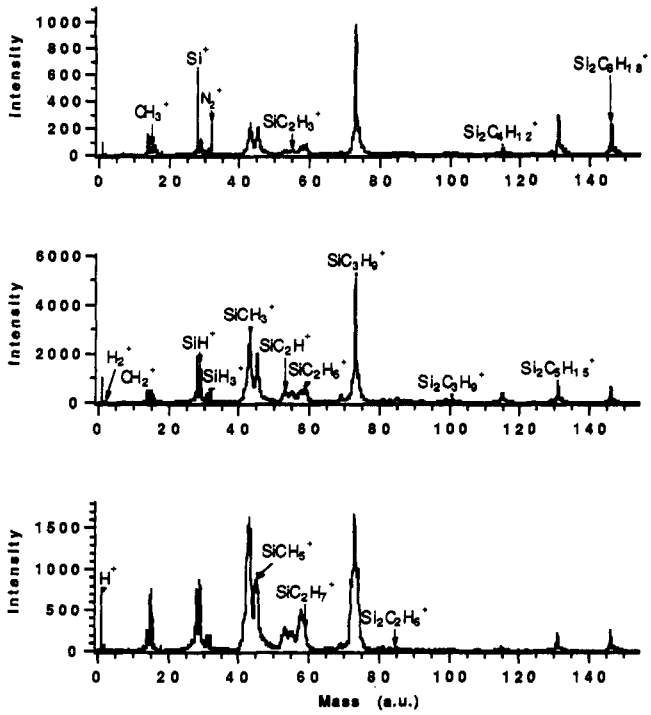

Figure 2. PEPICO spectra of HMDS recorded off resonance at 100 eV (top), on resonance 3 at 104.3 eV (center), and above threshold at 130 eV (bottom).

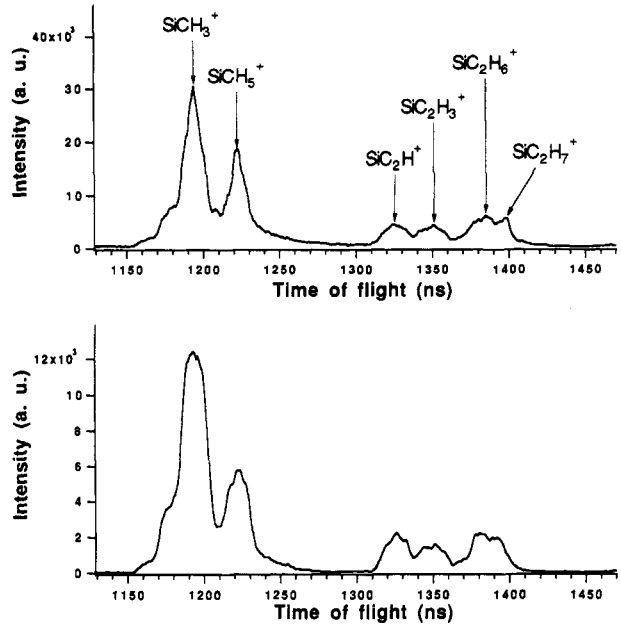

Figure 3. Part of the PEPICO spectrum (top) and PEPIPICO projection spectrum (bottom) showing the enlargement of the $SiCH_5^+$ and $SiC_2H_7^+$ peaks.

and another is formed. One sees that several concerted fragmentations or isomerizations are necessary to obtain the carbon substitution by hydrogen atoms. They are H_2^+, SiH^+, SiH_3^+, $SiCH_5^+$, and $SiC_2H_7^+$. The stability of SiH_3^+, SiH_2Me^+, and $SiHMe_2^+$ is sometimes explained by their trivalent structure:[11] they have an even number of electrons and are isoelectronic with the neutral stable group III molecules. We know, however, that it is dangerous to compare the bonding in carbon and silicon compounds.[23] It is very likely that the most stable valency of silicon is four rather than three. We will see below that this point may explain some rearrangement reactions.

It is interesting to note that the Si^+, SiH^+, and SiH_3^+ peak shapes are symmetric. This means that those rearrangement reactions are very fast on a microsecond time scale (typically less than 2 ns). On the other hand, the $SiCH_5^+$ and $SiC_2H_7^+$ peak shapes are asymmetric, to which we will now turn our attention.

An enlargement of the $SiC_2H_7^+$ and $SiCH_5^+$ peaks is given in Figure 3.

Asymmetric peaks in time-of-flight spectroscopy are a well-known signature of metastable ions.[24] Indeed, Chambers et al.[25] and De Ridder et al.[26] observed metastable $SiC_3H_9^+$ ions from Me_4Si and HMDS mass spectrometry. The following reactions were invoked

$$SiC_3H_9^+ \rightarrow SiC_2H_7^+ + :CH_2 \quad (1)$$

$$SiC_3H_9^+ \rightarrow SiCH_5^+ + C_2H_4 \quad (2)$$

but no lifetimes were measured.

In our experiment, metastable ion lifetime may be measured by comparing the actual peak shape with a simulated one. We have chosen $SiC_3H_9^+$ as a precursor, following the work of Gaidis et al.[27] Simulations of the present data were done within the following framework: we have assumed that the dissociation of the parent ion (singly or doubly charged) leading to $SiC_3H_9^+$ is a very fast process and that the $SiC_3H_9^+$ ion is slow to dissociate. Indeed, it may result from either single dissociative ionization or double dissociative ionization. Fortunately, as detailed in the next section, the peaks of the above-mentioned ions observed directly in double-ionization channels (PEPIPICO spectra) exhibit *exactly* the same asymmetric shape. We therefore conclude that in order to extract lifetimes measurement data, analysis can be done on one-dimensional spectra without corrections for spurious double coincidence event (see below).[14] In a metastable dissociation, the primary ion ($SiC_3H_9^+$ in our case) is first accelerated during a time τ in the interaction chamber. It then dissociates, and the resulting "daughter ion" is also submitted to the extraction field. A first-order calculation reveals that the time measured, t_{mes}, is given by $t_{mes} = TOF_{daughter} + (1 - m_d/m_p)\tau$, where $TOF_{daughter}$ is the daughter time of flight and m_d and m_p are respectively the mass of the daughter and of the $SiC_3H_9^+$ ion. This is a limiting case for very short lifetimes. The dispersion in the time of dissociation can be determined by measuring the ion's time-of-flight distribution. We now analyze the asymmetric time-of-flight (TOF) peak shape in terms of the dissociation rate.

We show in Figure 4 the detailed peak shapes of $SiC_2H_5^+$ and $SiC_2H_7^+$: the experimental points are fitted with calculated time-of-flight distribution, in which the only adjustable parameters are the ion dissociation rate and the width of the time-of-flight distribution. This width is due to the instrumental resolution and the kinetic energy released in the dissociation. These effects are taken into account by convoluting the decay function with a Gaussian function.

We obtained the best fit with the following decay times:

$$SiC_2H_7^+ \qquad T = 45 \pm 5 \text{ ns}$$

$$SiCH_5^+ \qquad T = 49 \pm 5 \text{ ns}$$

We used a single-exponential decay because the experimental results are well fitted in those conditions. In fact, this must be an average value over several times. Since both are produced from the same ion, it seems more reasonable to assume two competing processes and to model the line shape by a double-exponential decay. The similarity of the two lifetimes within the error bars shows that a single-exponential decay is sufficient to correctly fit the data.

The observation of rearranged fragment ions is compatible with a fast cleavage of the Si–Si bond followed by a slow fragmentation decay of the $SiC_3H_9^+$ ion. We suspect that it

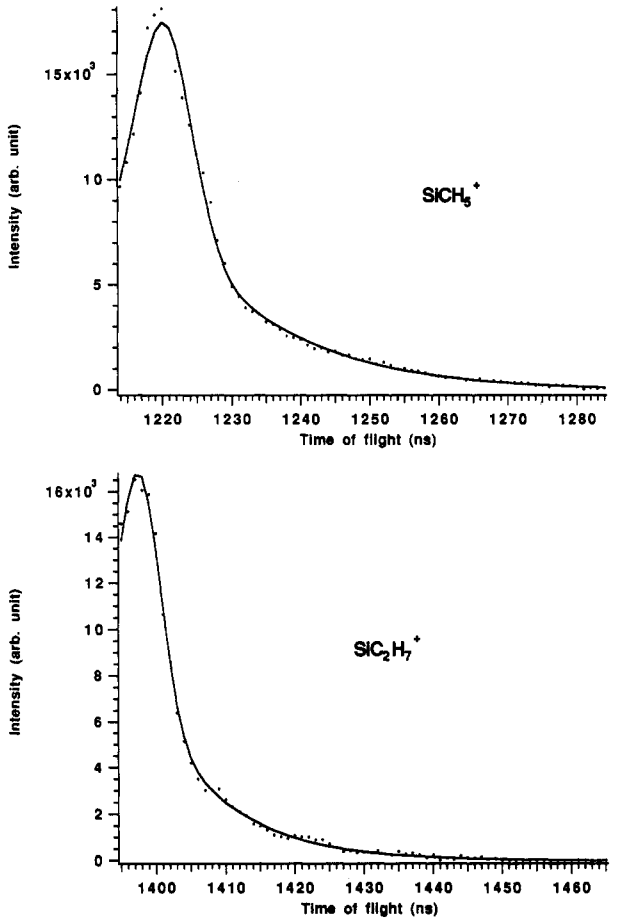

Figure 4. Time of flight of SiH_2Me^+ and $SiHMe_2^+$ spectra. Dots represent the experimental data, and the curve is the best fit of the lifetime using single-exponential decay.

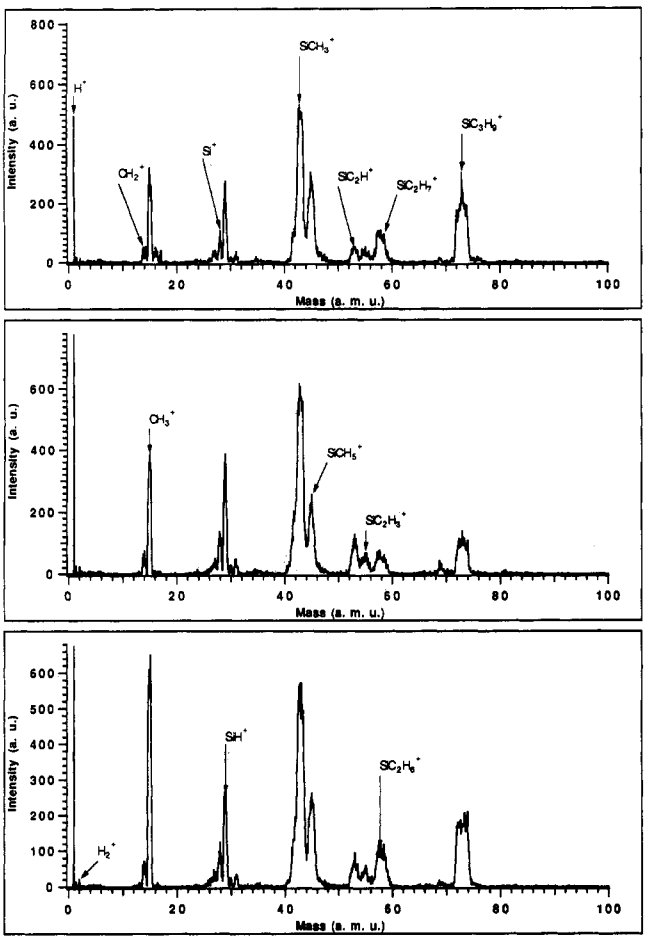

Figure 5. PEPIPICO projection spectra recorded off resonance at 100 eV (top), on resonance 3 at 104.3 eV (center), and above threshold at 130 eV (bottom). These spectra represent the dissociation spectra of the multiply charged ($n \geq 2$) HMDS molecule.

isomerizes into a tetravalent form before ejecting CH_2. Successive steps of this kind provide substitution of methyl ligands by hydrogen.

Double-Ionization Dissociation Spectra

PEPIPICO Projection Spectra. In the PEPIPICO data, the time of flight of the two ions issuing from a dissociative double-ionization event t_1 and t_2, are recorded simultaneously. They correspond to the arrival of two correlated ions during the time window open after one-electron detection. Data are stored as (t_1,t_2,z), where $z(t_1,t_2)$ is the number of occurrences of the couple (t_1,t_2). We drop all triplets with $z = 1$, which are considered as random background noise. This saves a lot of computer memory but has to be avoided in the quest of very low signal. We project peaks along the two axes t_1 and t_2 and sum those two projections. The resulting PEPIPICO projection spectra show the yield of ions created in coincidence with one other charged fragment. Because the ion detection efficiency is lower than 1, these spectra contain the contibution of dissociative double ionization as well as contribution of dissociative triple ionization, where only two ions have been detected. Notice that there is no contribution of dissociative single-ionization events. We present in Figure 5 PEPIPICO projection spectra of HMDS recorded at selected wavelengths: below resonance 3, on resonance 3, and above the Si 2p ionization edge.

The heaviest observed fragment is $SiC_3H_9^+$. The absence of ion as $Si_2C_xH_y^+$ ($x = 0, 6$; $y = 0, 18$) in those double-ionization projection spectra proves that double ionization involves systematically the Si–Si chemical bond cleavage.

The main fragments are $SiCH_3^+$ and $SiCH_5^+$: they result from multiple bond cleavage. The ratio of light fragments is more important in double-ionization projection spectra than in simple coincidence spectra, showing the importance of many-body fragmentation.

As can be seen in Figure 5, the fragmentation resulting from double coincidence increases with increasing photon energy. This may be due to the triple-ionization contribution, whose cross section increases with photon energy.

We notice that in PEPIPICO projection spectra SiH^+ formation is more important than Si^+ and also that CH_3^+ is more important than CH_2^+. This means that doubly charged ions dissociate predominantly in SiH^+ and CH_3^+ instead of Si^+ and CH_2^+. It is exactly the opposite of what is observed below threshold. At higher photon energy, SiH^+ and CH_3^+ peak intensity increases, which is probably due to a higher double-ionization contribution in PEPIPICO spectra (see below).

It is remarkable that $SiCH_5^+$ and $SiC_2H_7^+$ peak shapes are exactly the same in PEPICO spectra and in PEPIPICO projection spectra. This is illustrated in Figure 3, where the same region of time of flight has been reported. We simulated spurious coincidence (see below) from metastable data (not shown), and we concluded that metastable ions are due both from single- and double-ionization events. The shape similarity indicates that the $SiC_3H_9^+$ ions formed by either simple or double ionization follow the same metastable decay route. This results in the PEPIPICO spectra, in vertical or horizontal "tracks" following the $SiCH_5^+$ and SiC_2H^{7+} time of flight. Such a feature can be seen in Figure 11.

Contribution of Double Ionization in Simple Coincidence Spectra. Because of experimental conditions (ringing in the ion signal), we have to set a relatively high discrimination level to the ion signal in order to operate double-coincidence measurements. We know[14] that under such conditions we discriminate against

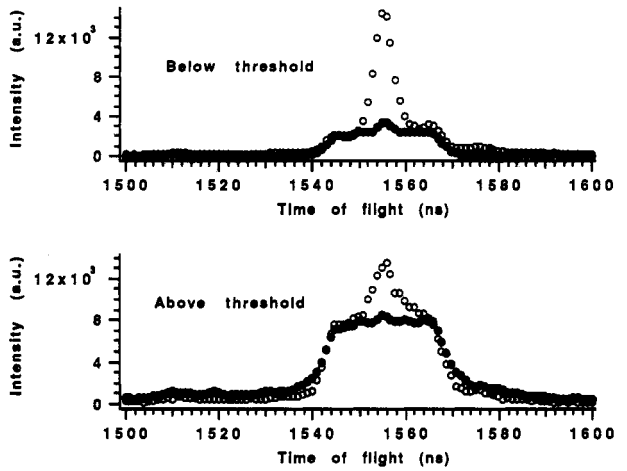

Figure 6. $SiC_3H_9^+$ ion peak in the simple coincidence spectrum below and above the Si 2p threshold. Open circles correspond to the simple coincidence measured; solid circles correspond to the calculated spurious double coincidences (see text). The small peak in the center of the spurious double coincidence spectrum is due to false double coincidences.

TABLE II: Double/Single Ionization Ratio Producing the $SiC_3H_9^+$ Ion

photon energy (eV)	σ^{2+}/σ^+ dissociating into $SiC_3H_9^+$	photon energy (eV)	σ^{2+}/σ^+ dissociating into $SiC_3H_9^+$
100 (below resonances)	0.72	104.3	1.19
103.1	0.97	104.8	2.22
103.9	1.16	130 (above threshold)	7.14

heavy ions: the ion detection efficiency is a decreasing function of the ion detected mass. Thus we cannot subtract easily from single-ionization spectra the contribution of dissociative multiple ionization where only one ion has been detected. We have determined the ion detection efficiency as a function of mass by comparing simple coincidence spectra taken at low- and high-discrimination levels assuming no mass discrimination at low level. Knowing the ion detection efficiency and the PEPIPICO data, we then built up the "spurious coincidence spectrum". It represents the contribution of dissociative multiple ionization which reduces to a one-dimensional spectrum because only one ion has been detected. The detailed procedure is explained in the Appendix.

The comparison between simple coincidence and calculated spurious coincidence spectra for $SiC_3H_9^+$ ion is shown in Figure 6 at two photon energies: below and above the Si 2p threshold.

Figure 6 shows that the spurious double-coincidence peak is broad due to a large amount of kinetic energy released. The simple coincidence spectrum of the $SiC_3H_9^+$ peak contains this broad enhancement added to a narrow Gaussian peak due to lower kinetic energy released in the dissociation of singly charged ions. Comparison of the two photon energy spectra in Figure 6 proves that dissociative multiple ionization is much more efficient above the Si 2p threshold than below. Note that our correction procedure seems to be quite correct. Indeed, in this favorable situation, we can estimate the spurious coincidences from the difference in the amount of kinetic energy release. The calculated spectrum exactly matches this contribution. The double/single ionization ratios producing $SiC_3H_9^+$ are listed at six photon energies in Table II.

It clearly shows that the cross section of double-ionization events producing $SiC_3H_9^+$ ion increases with photon energy at each resonance. We can reasonably assume that it is the case for the total double-ionization cross section. In the case of the Si 2p ionization continuum, this is due to relaxation through normal Auger decay, which leads to double ionization and not to single ionization.

Dissociation Dynamics of Doubly Charged Ions

Model. In this part, we study the dissociation dynamics of a doubly charged molecule through the analysis of the coincidence peak shape within the t_2 vs. t_1 plot.

Two-Body Ion Pair Processes. Let us consider the AB^{2+} dissociation into $A^+ + B^+$. If we neglect thermal velocity before dissociation, momentum conservation law induces anticorrelation between the kinetic momenta of A and B: $p_A = -p_B$. Under space-focusing conditions, at first order, the time of flight t for any ion is given by $t = t^0 - kp_\parallel$ where t^0 is the flight time for any ion starting at rest, $p_\parallel$ is the initial kinetic momentum projection toward the detector axis, and k is a geometrical constant which includes the extracting electrostatic field. In PEPIPICO spectra, we plot the time of flight of the second ion, t_2, versus the time of flight of the first ion, t_1. Because of the anticorrelation of the kinetic momenta, if we neglect the constant part in the time-of-flight expression (which only changes the origin of the peaks), we obtain $t_2 = -t_1$, which results in a short segment in the t_2 vs. t_1 plot, oriented at 45°. Its length reflects the kinetic energy release in the dissociation. One can change the initial t_2 vs t_1 plot into $t_2 - t_1$ vs $t_2 + t_1$, which transforms the peak into a horizontal segment. Unfortunately, most of the polyatomic doubly charged molecule dissociation involves several chemical bond cleavages. Therfore, we have to consider three- and four-body ion pair processes.

Three-Body Ion Pair Processes. We now consider the cleavage of two chemical bonds

$$ABC^{2+} \rightarrow A + B^+ + C^+$$

and the important question we want to answer concerns the sequentiality or simultaneity of the two bond breakings. We have to distinguish three dissociation mechanisms, as first introduced by Eland:[28] (1) deferred charge separation (DCS), where a neutral particle is first ejected, followed in a second step by charge separation of the two charged fragments; (2) secondary decay (SD), where a fragment ion is first ejected, followed by dissociation of the remaining ion; and (3) concerted three-body dissociation, where at least two bonds break simultaneously.

It is important at this point to specify the time scale when stepwise processes are involved. We suppose the time scale large enough so that dissociation energies can be defined and that kinetic momentum conservation can be applied at each step.

By neglecting the kinetic energy release in the step corresponding to the neutral ejection, Eland[28] early demonstrated that the slope of the peak in the PEPIPICO spectrum gives the sequentiality information. Later, by Monte Carlo simulation,[13] he obtained parallelogram peak shape in the PEPIPICO spectrum. We want to determine analytically the peak shape in the PEPIPICO spectrum of those two processes, to extract from the peak shape the corresponding process, and furthermore to measure the kinetic energy release in the two steps.

(*a*) *Deferred Charge Separation.* We consider the following mechanism:

$$ABC^{2+} \rightarrow A + BC^{2+} \quad (U_1)$$

$$BC^{2+} \rightarrow B^+ + C^+ \quad (U_2)$$

We note that $\mathbf{p}$ is the kinetic momentum vector of A after dissociation. U_1 is the kinetic energy released in this dissociation. From energy conservation, we can write

$$\mathbf{p}^2 = \frac{2U_1 m_A (m_{B^+} + m_{C^+})}{m_A + m_{B^+} + m_{C^+}}$$

We note that $\mathbf{q}$ is the kinetic momentum of B^+ after the second dissociation, in the BC^{2+} frame. If U_2 is the kinetic energy released

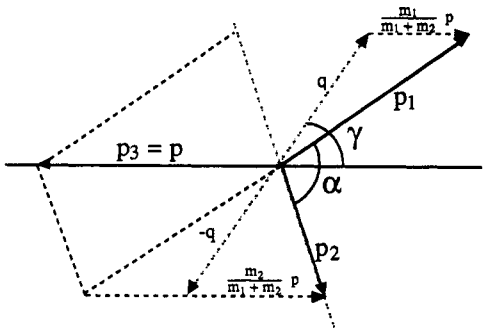

Figure 7. Definition of angles and kinetic momenta.

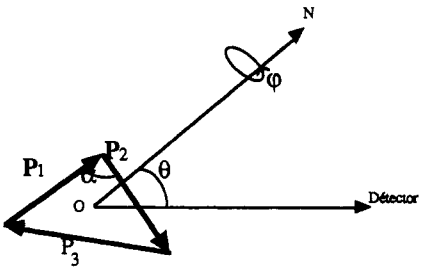

Figure 8. Orientation of the dissociation plane.

corresponding to this second dissociation, we have

$$\mathbf{q}^2 = \frac{2U_2 m_{B^+} m_{C^+}}{m_{B^+} + m_{C^+}}$$

We neglect now U_1 with respect to U_2, and because the second step corresponds to the Coulomb repulsion, we obtain $p_{A^+} = 0$ and $p_{B^+} = -p_{C^+}$, and the peak will be a narrow peak of slope −1 in the ion–ion time deviation regression, as in the case of two-body dissociation. We explain below the full theoretical treatment if U_1 is not small compared to U_2.

$$\mathbf{p}_1 = \mathbf{p}_A = \mathbf{p}$$

$$\mathbf{p}_2 = \mathbf{p}_{B^+} = \mathbf{q} - \frac{m_{B^+}}{m_{B^+} + m_{C^+}}\mathbf{p}$$

$$\mathbf{p}_3 = \mathbf{p}_{C^+} = -\mathbf{q} - \frac{m_{C^+}}{m_{B^+} + m_{C^+}}\mathbf{p}$$

We have introduced **p** and **q**, variables of physical interest but not directly relevant for t_2 vs t_1 plots. We also can introduce a third parameter of interest: the angle γ between **p** and **q** (see Figure 7).

γ measures the rotation of the BC^{2+} axis before the second dissociation takes place. In the general case, this angle is not a fixed parameter but may have a density distribution. $\mathbf{p}_{B^+}$ and $\mathbf{p}_{C^+}$ may be written explicitly as a function of γ:

$$\mathbf{p}_{B^+}{}^2 = \mathbf{q}^2 + \left(\frac{m_{B^+}}{m_{B^+} + m_{C^+}}\mathbf{p}\right)^2 - 2(\cos\gamma)\mathbf{pq}\frac{m_{B^+}}{m_{B^+} + m_{C^+}}$$

$$\mathbf{p}_{C^+}{}^2 = \mathbf{q}^2 + \left(\frac{m_{C^+}}{m_{B^+} + m_{C^+}}\mathbf{p}\right)^2 + 2(\cos\gamma)\mathbf{pq}\frac{m_{C^+}}{m_{B^+} + m_{C^+}}$$

To obtain t_1 and t_2, we take the projections of $\mathbf{p}_{B^+}$ and $\mathbf{p}_{C^+}$ along the detection axis. Since $p_A + p_B + p_C = 0$, dissociation of the molecule takes place in a plane, and the three momenta form a triangle. Its orientation with respect to the detection axis is given by the angles θ and φ.

As labeled on Figure 8, θ is the angle between the normal of the plane and the detector axis and φ is the angle corresponding to any rotation of the triangle around the normal. We call α the angle between $\mathbf{p}_B$ and $\mathbf{p}_C$. We obtain for the projection $p_\parallel$[29]

$$\mathbf{p}_{B\parallel^+} = \mathbf{p}_{B^+} \cos\varphi \sin\theta$$

$$\mathbf{p}_{C\parallel^+} = \mathbf{p}_{C^+} \cos(\varphi + \alpha) \sin\theta$$

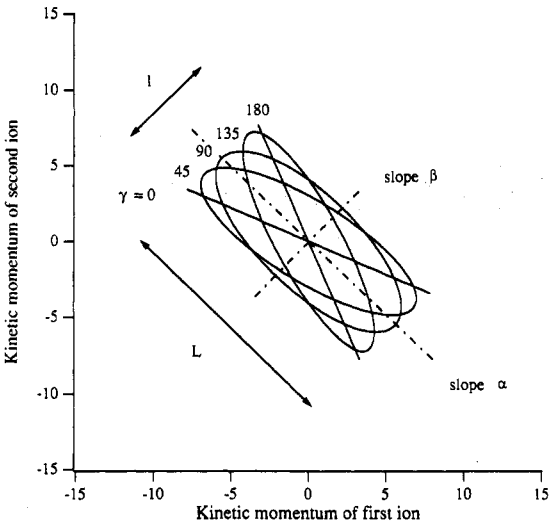

Figure 9. Parallelogram obtained after a DCS process at various γ angles, corresponding to the rotation of the fragment prior to the second dissociation. $\alpha = -1$, $\beta = m_C/m_B$, $l = p$, and $L = [((m_C{}^2 + m_B{}^2)/(m_C + m_B))q]^{1/2}$.

These two equations define a parametric representation of various ellipses. For a given dissociation process (U_1, U_2, and γ are fixed), p_B and p_C are given by these equations and the t_2 vs t_1 plot is a set of homothetic ellipses described by varying φ. The size of the ellipse is given by the choice of θ. When $\theta = 0$ (dissociation perpendicular to the detection axis), the ellipse reduces to a point corresponding to particles initially at rest ($t_1{}^0$,$t_2{}^0$). When $\theta = 90°$ (ejection along the detection axis), the plot is an ellipse of maximal size. Because of initial random orientation of molecules before ionization, θ can take any value between 0 and 90°, which means that the t_2 vs t_1 plot is a filled ellipse whose size is given by the kinetic energy released. For clarity, in the following, we only discuss the external contour of filled ellipses.

The interesting point is to obtain the final t_2 vs t_1 plot as a function of the γ parameter. We show in Figure 9 calculations of the t_2 vs t_1 plot for various dissociation angles γ.

The effect of the rotation γ before dissociation of BC^{2+} is to rotate the ellipse. From this, we deduce that if the fragment BC^{2+} has time to rotate several turns before it dissociates, the angle γ can take any random value between 0 and 180°, and the result is that the t_2 vs t_1 plot is a parallelogram of well-defined orientation and size, illustrated in Figure 9 (where α, β, l, and L are defined).

We thus deduce that, in the case of DCS, the expected figure is a parallelogram of slope −1, whose size measures the kinetic energy released in each step. We define slope as the slope side of the parallelogram (explained in Figure 9). The figure is the same as the one obtained by Eland[13] using Monte Carlo simulation to reproduce PEPIPICO spectra. We have used very high electrostatic field in the ionization chamber (2000 V/cm) in order to reduce discrimination against energetic ions. This means that the peak shape is small, and the kinetic energy release determination is obtained with more uncertainty than that obtained with a lower field.

Recently, Lavollée and Bergeron[30] demonstrated that transformation into the reduced variables $X = t_1 + t_2$ and $Y = (m_C t_1 - m_B t_2)/(m_B + m_C)$ transforms the t_2 vs t_1 plot into a rectangle whose lengths are respectively $|\mathbf{p}|$ and $|\mathbf{q}|$ (the problem variables

of physical interest) and oriented parallel to the X and Y axes. Thus, to measure **p** and **q** we just have to use the reduced variables. The projection toward the X axis gives a peak of width kp and toward the Y axis a peak of width kq, where k is a geometric factor. It must be calibrated when absolute energy has to be measured.

(*b*) *Secondary Decay.* We consider now the following mechanism:

$$ABC^{2+} \rightarrow B^+ + AC^+$$

$$AC^+ \rightarrow A + C^+$$

The mathematical modeling of this process is very similar to the deferred charge separation process. We note simply that the two detected particle are $\mathbf{p}_1$ and $\mathbf{p}_2$ instead of $\mathbf{p}_2$ and $\mathbf{p}_3$.

In this case, the correlation plot t_2 vs t_1 is also a parallelogram with one side vertical or horizontal depending on whether the heaviest particle is B^+ or C^+. Similarly, the other side of the parallelogram has a slope equal to the mass ratio $-m_C/(m_A + m_C)$ or $-(m_A + m_C)/m_C$ depending on whether the heaviest detected mass is B^+ or C^+. The use of reduced variables[30] $X = t_2$ and $Y = t_1 + m_A t_2/(m_A + m_C)$ transforms the PEPIPICO peak into a rectangle whose lengths are respectively equal to **q** and **q**. It is important to notice that there are two variable changes depending on whether B^+ or C^+ is the heaviest detected particle. By Monte Carlo simulation, Eland[13] obtained exactly the same results.

As a conclusion for this section, we have pointed out two possibilities to determine the dissociation mechanism: (1) determination of the slope of the parallelogram (we explain the procedure followed in the next section) and (2) trying the various coordinate transformations previously described an comparing the corresponding two-dimensional plot. A rectangle is obtained, with sides parallel to the X and Y axes, only if the dissociation mechanism follows one of the already described processes.

For the two processes SD and DCS, Lavollée and Bergeron[30] were able to determine theoretically the γ density distribution of a peak. However, in this case, it was not possible because of insufficient statistics and also because of eventual anisotropy in the ejection of the ions.

(*c*) *Concerted Dissociation.* In such a process, the kinetic momenta distribution among the three particles is not necessarily unique, and this is likely to result in an ovoid peak, especially if the momenta are not aligned (Eland[31]).

As we will see below for HMDS, the three-body ion pair processes explain most of the measured peaks. However, occasionally we must consider four-body ion pair processes to extract the dissociation mechanism.

Four-Body Ion Pair Processes. We now consider the $ABCD^{2+}$ dissociation into $A + B^+ + C^+ + D$. In the same way as for the three-body ion pair processes, we try to obtain a signature of stepwise mechanism revealed by the peak shape.

(*a*) *Deferred Charge Separation.* We consider in this case the following mechanism in three different steps:

$$ABCD^{2+} \rightarrow ABC^{2+} + D$$

$$ABC^{2+} \rightarrow BC^{2+} + A$$

$$BC^{2+} \rightarrow B^+ + C^+$$

This process cannot be distinguished, of course, from the one where AD is lost in a first step. Consequently, it results in a parallelogram plot, with a -1 slope.

(*b*) *Secondary Decay.* This case corresponds exactly to the three-body secondary decay with the loss of AD instead of A.

$$ABCD^{2+} \rightarrow ACD^+ + B^+$$

$$ACD^+ \rightarrow AC^+ + D$$

$$AC^+ \rightarrow A + C^+$$

Thus, the associated peak shape is a parallelogram with a horizontal or vertical side and a slope equal to $-m_C/(m_A + m_C + m_D)$ or $-(m_A + m_C + m_D)/m_C$, respectively, when B^+ or C^+ is the heaviest.

Secondary Decay after a Deferred Charge Separation.

$$ABCD^{2+} \rightarrow ABC^{2+} + D$$

$$ABC^{2+} \rightarrow AB^+ + C^+$$

$$AB^+ \rightarrow A + B^+$$

The first step can be considered as a step producing an isotropic kinetic momentum to a doubly ionized triatomic molecule which dissociates following a secondary decay. So, as for the secondary decay of three-body ion pair processes, the peak shape is a parallelogram with a horizontal or vertical side and a slope equal to $-m_B/(m_A + m_B)$ or $-(m_A + m_B)/m_B$ for B^+ or C^+ heaviest. For this mechanism, we can affirm that the dissociation takes place in three different steps, which is not the case for the two previously studied processes.

Secondary Decay in Competition.

$$ABCD^{2+} \rightarrow AB^+ + CD^+$$

$$AB^+ \rightarrow A + B^+$$

$$CD^+ \rightarrow C^+ + D$$

As was suggested by Eland,[28] if we neglect the kinetic energy release corresponding to the neutral ejection, we directly obtain that the associated shape of the peak is a parallelogram with a slope equal to $-(m_B/(m_A + m_B))/(m_C/(m_C + m_D))$ or $-(m_C/(m_C + m_D))/(m_A/(m_A + m_B))$ for B^+ or C^+ heaviest. The process certainly occurs in three different steps. In this case, we are sure that A and D are not chemically bonded.

Concerted Dissociation.

$$ABCD^{2+} \rightarrow A + B^+ + C^+ + D$$

This process is unlikely, but the chemical bond rupture can be so fast that we cannot distinguish experimentally the different step. Another reason can also be due to the fact that the dissociation is so fast that the four particles are still in interaction during the bond breaking.

We have not considered all the four-body ion pair processes where two steps are simultaneous and the third one deferred.

Application to the HMDS Peaks. *General Overview of PEPIPICO Spectra.* There are about 40 peaks in the PEPIPICO spectra corresponding to 40 different ion pairs. One of the advantages of the PEPIPICO method, compared to the PIPICO method, is the measurement of the absolute time of flight of the ions rather than the time-of-flight differences, so that ambiguities in assigning peaks are removed. An example is given in Figure 10, where the different ions are identified.

Branching Ratio of the Different Dication Pair Processes. The cross sections were summed over all photon energies because no selectivity was seen: the results are independent of photon energy. In order to increase the statistics, we add all the PEPIPICO spectra recorded at the different photon energies and calculate the volume of double coincidence of each pair. The results are listed in Table III.

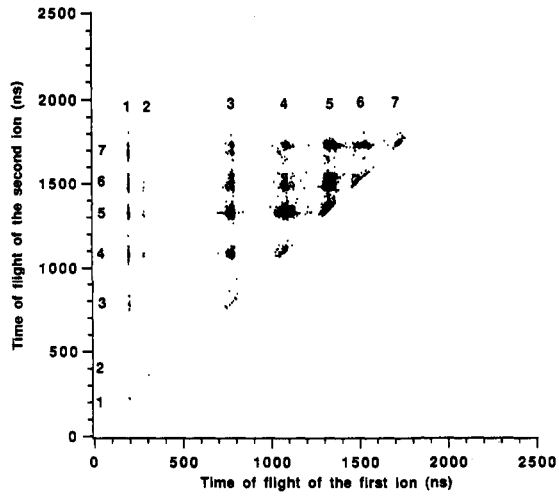

Figure 10. General overview of PEPIPICO spectrum. We have labeled seven groups of peaks with the following assignments: 1, H^+; 2, H_2^+; 3, CH_i^+; 4, SiH_i^+; 5, $SiCH_i^+$; 6, $SiC_2H_i^+$; 7, $SiC_3H_i^+$.

We define the volume of a given ion pair as the total number of counts within the peak corresponding to this pair. The volume of the CH_2^+/CH_2^+ pair is not indicated because of N^+/N^+ contribution due to a small leak in the gas introduction system.

Since $SiC_3H_9^+$ is the heaviest ion in the PEPIPICO spectrum, only the $SiC_3H_9^+/SiC_3H_9^+$ pair can be considered as a two-body ion pair process. Due to the dead time (≈7 ns) between the arrival of two successive ions, we do not have the complete signal of this pair. If we project this peak toward the $t_1 + t_2$ axis, we obtain an experimental width which is due to both thermal velocity of the parent molecule in the effusive jet of gas[31] and instrumental width. This width is equal to the width of the parent ion in the simple coincidence spectrum (4 ns). The projection of this peak toward the $t_2 - t_1$ axis gives the kinetic momentum release during the dissociation. By assuming that the kinetic momentum distribution is unique, we can recover the whole peak shape of the projected peak by adding the missing points due to the dead time. Thus we can obtain the volume of this pair.

The same procedure was used to measure the volume of all symmetric pairs.

Determination of the Dissociation of the Selected Pairs. (*a*) *Selected Pairs.* We select the most predominant of the peaks and especially those which contain the $SiC_3H_9^+$ ion (there are 40 in all). We are interested with the series Me^+, SiH^+, $SiCH_3^+$, $SiCH_5^+$, and $SiC_2H_6^+$ in coincidence with $SiC_3H_9^+$. We also focus on the $CH_3^+/SiCH_3^+$ peak because of its particularly high cross section. The corresponding peaks are presented in Figure 11.

It is striking to observe that all these peaks, except that in coincidence with Me^+, are described by a parallelogram. This shows two important points concerning the dynamics: (1) dissociative double ionization is dominated by stepwise processes (secondary decay) and (2) in each case, only one specific dissociation decay is observed (otherwise we would observe a superposition of parallelograms of different slopes).

Figure 11 clearly shows that the slope of the different peaks increases from the $SiC_2H_6^+/SiC_3H_9^+$ pair up to the $SiH^+/SiC_3H_9^+$ pair. For the $SiCH_3^+ + /SiC_3H_9^+$ pair, the slope is lower and the peak is larger. For the peak $CH_3^+/SiCH_3^+$, the peak is very large and resembles more an "egg" than a "cigar".

(*b*) *Procedure for Mechanism Determination.* As explained in the previous subsection, there are two possibilities to determine the mechanism followed during the dissociative double-ionization processes. Because we know the two times of flight we can assign the two detected ions, and we know the mass of the undetected particle(s). So it is easy to consider a two-, three-, four-, or many-body ion pair process. We used both the slope determination procedure and the best variable change procedure which transforms the parallelogram into a rectangle. For all pairs checked, we obtain always the same mechanism: the rectangle peak perfectly matches the mechanism associated to the measured slope. The variable change procedure has the advantage that it gives information about the kinetic momenta release during the two steps: neutral ejection and charge separation. For the slope determination, the only adjustable parameter is the straight line slope which is determined by least-squares fit of the distance between the straight line and the point (t_1,t_2) weighted by its occurrence $z(t_1,t_2)$.

We determined the slopes of the parallelogram of the six selected peaks at the different photon energies of the resonances and found always the same value. It shows that the dissociation processes are not energy dependent. Therefore, we summed the spectra recorded at all photon energies, thus improving the statistics, and obtained a slope with a smaller uncertainty. The results are listed in Table IV with measured slope, the proposed associated mechanism, and its corresponding calculated slope.

For SiH^+, $SiMe^+$, $SiCH_5^+$, and $SiC_2H_6^+$ in coincidence with $SiC_3H_9^+$, we found the same mechanism: secondary decay with a first step consisting of the dissociation of $HMDS^{2+}$ into two $SiC_3H_9^+$ ions. It shows that the Si–Si chemical bond rupture always occurs before the Si–C rupture. With this model, we cannot calculate the time scale of the different processes, but we can reasonably estimate that the Si–Si rupture occurs in less than 1 ps. The observation of a regular parallelogram probably indicates that the Si–C rupture occurs after several rotations of the fragment. In other words, the lifetime of $SiC_3H_9^+$ is long compared to its rotation.

(*c*) *Momenta Release during the Two Steps.* After mechanism determination, we transformed the PEPIPICO peak with the reduced variables following the procedure explained in the previous subsection, and we obtained a rectangle whose length corresponds to the two kinetic momenta **p** and **q** of the two steps. In Table V we list the measured kinetic momenta of the two steps.

It is interesting to notice that all pairs are associated with the same **p** value: the projection of the peak with reduced variables gives a shape which is the convolution of a Gaussian of 4-ns fwhm and a rectangle 20 ns broad. Four nanoseconds is exactly the fwhm of the following two peaks: the parent ion in the simple coincidence spectrum and the $SiC_3H_9^+/SiC_3H_9^+$ PEPIPICO peak projected toward the $t_1 + t_2$ axis. We calculated the kinetic energy release corresponding to this width. The similarity of all these widths suggests that the first dissociation step is the same for all processes.

For the $CH_3^+/SiC_3H_9^+$ peak, we cannot propose a mechanism for two reasons: (1) the peak is ovoid and can be due to a fast explosion of the doubly charged molecule and (2) the dissociative triple ionization mainly produces the pair $CH_3^+/SiC_3H_9^+$. So the peak measured in the PEPIPICO spectrum contains both contribution from double ionization and triple ionization where one ion has not been detected. It is interesting to note that triple ionization occurs on a time scale faster than double ionization, giving an ovoid peak interpreted as an instantaneous explosion.

Conclusion. Double ionization of HMDS is dominated by stepwise dissociation channels. The Si–Si chemical bond cleavage always occurs before any Si–C chemical bond cleavage. This fact is observed both for singly[17] and doubly charged molecules. The kinetic energy release of the first step does not depend on the dissociation(s) that follow.

Bond-Selective Fragmentation

We now consider the absence of bond-selective fragmentation. We distinguish bond-selective processes at a given core level edge from site-selective process (comparison of different ionization edges with the same unoccupied orbitals). In the first case, the similarity between resonance 1 and resonances 2–6 may be

TABLE III: Volume[a] of Double Coincidence Electron–Ion–Ion Measured for all the Summed PEPIPICO Spectra

ion	H^+	H_2^+	CH_2^+	CH_3^+	Si^+	SiH^+	SiH_3^+	$SiMe^+$	SiH_2Me^+	$SiMe_2^+$	$SiHMe_2^+$	$SiMe_3^+$
H^+	0	0	94	475	1056	1656	161	30409	879	132	158	464
H_2^+		0		46	47	0	179	0	0	0	0	0
CH_2^+					245	524	32	1514	0	0	0	0
CH_3^+					1154	3657	379	14017	2718	2092	1373	1812
Si^+					0	1060	98	4623	0	0	0	657
SiH^+						0	519	10721	3238	909	0	3382
SiH_3^+							0	1473	382	49	41	291
$SiMe^+$								20226	9180	1848	924	11234
SiH_2Me^+									6522	2706	2224	6840
$SiMe_2^+$										1101	0	9049
$SiHMe_2^+$											0	0
$SiMe_3^+$												10941

[a] Volume of a given ion pair is defined as the total number of counts within the peak corresponding to this pair.

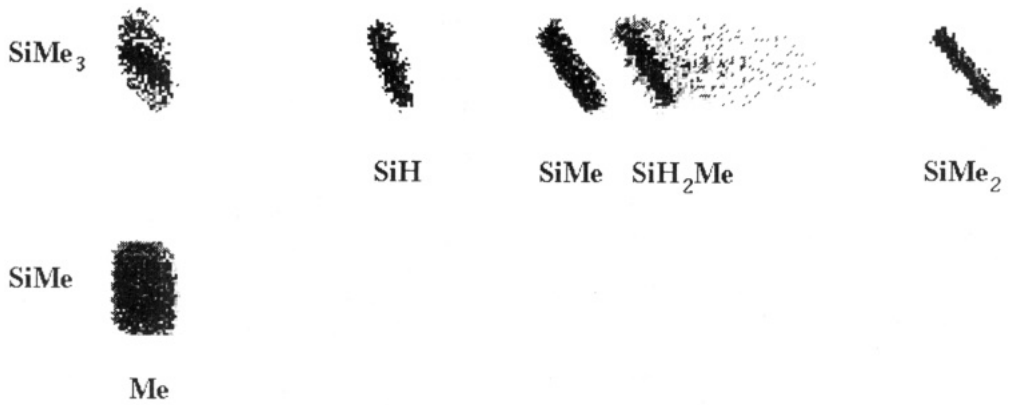

Figure 11. Selected pairs of the PEPIPICO spectrum of HMDS. The two arrival times of the first and second ion, t_1 and t_2 are the coordinates in the plane, and the intensity is given in false color.

TABLE IV: Proposed Mechanism for Selected Ion Pairs Arising from HMDS Double-Coincidence Spectra

pair	measd slope	mechanism	calcd slope
$Me^+/SiMe_3^+$	−0.71	concerted?	?
$SiH^+/SiMe_3^+$	−2.52	$HMDS^{2+} \rightarrow 2SiC_3H_9^+$ $SiC_3H_9^+ \rightarrow SiH^+ + C_3H_8$	−2.50
$SiMe^+/SiMe_3^+$	−1.65	$HMDS^{2+} \rightarrow 2SiC_3H_9^+$ $SiC_3H_9^+ \rightarrow SiMe^+ + C_2H_6$	−1.7
$SiH_2Me^+/SiMe_3^+$	−1.60	$HMDS^{2+} \rightarrow 2SiC_3H_9^+$ $SiC_3H_9^+ \rightarrow SiH_2Me^+ + C_3H_6$	−1.62
$SiMe_2^+/SiMe_3^+$	−1.23	$HMDS^{2+} \rightarrow 2SiC_3H_9^+$ $SiC_3H_9^+ \rightarrow SiMe_2^+ + Me$	−1.26
$Me^+/SiMe^+$	−0.71	$HMDS^{2+} \rightarrow SiC_3H_9^{2+} + SiC_3H_9$ $SiC_3H_9^{2+} \rightarrow Me^+ + SiMe_2^+$ $SiMe_2^+ \rightarrow SiMe^+ + Me$	−0.74

TABLE V: Kinetic Momenta Determined for Each Dissociation Step of the Selected Ion Pairs[a]

pair	mechanism		
$SiH^+/SiC_3H_9^+$	$HMDS^{2+} \rightarrow 2SiC_3H_9^+$ $SiC_3H_0^+ \rightarrow SiH^+ + C_3H_8$	20	8
$SiCH_3^+/SiC_3H_9^+$	$HMDS^{2+} \rightarrow 2SiC_3H_9^+$ $SiC_3H_9^+ \rightarrow SiCH_3^+ + C_2H_6$	20	7
$SiCH_5^+/SiC_3H_9^+$	$HMDS^{2+} \rightarrow 2SiC_3H_9^+$ $SiC_3H_9^+ \rightarrow SiCH_5^+ + C_2H_4$	20	8
$SiC_2H_6^+/SiC_3H_9^+$	$HMDS^{2+} \rightarrow 2SiC_3H_9^+$ $SiC_3H_9^+ \rightarrow SiC_2H_6^+ + Me$	?	?

[a] The kinetic momenta are expressed in ns; the conversion to eV can easily be obtained by following the formula $KE(eV) = 4.82 \times 10^{-5}/m[E(V/mm)\Gamma(ns)]^2$.

interpreted in terms of "delocalization" of the core-excited electron over the whole molecule. This should be confirmed by calculations. In such a case, the concept of bond-selective fragmentation expected from the "localized" picture of Sette et al.[16] is wrong. Secondly, even if resonance 1 had a dominant Si–Si antibonding character and resonances 2–6 are mostly Si–C antibonding, the electronic decay (resonant Auger) may keep the charge localized in the initially excited bond, but the cascade of fragmentation processes leads to the same intermediate ion (e.g., $SiC_3H_9^+$). This ion is produced with a large distribution of internal energy. This explains why this ion is found stable on a microsecond time scale or seen through fragments. Furthermore, its isomerization prior to framentation was shown. In summary, this $SiC_3H_9^+$ ion fragmentation behaves in a "normal" statistical way, independent of the mechanism of its production. This has to be checked theoretically. Therefore, even if the initial excitation is localized, the system loses its memory on a microsecond time scale because the same long-lived fragment ion is always produced. Notice that a bond-selective process would have meant the absence of vibrational redistribution at, at least, one stage of fragmentation. In fact, if one stage is statistical, what follows will reflect the selectivity at this stage. In other words, the dissociation step not statistical would proceed through fast repulsive surfaces. Such hypothesis is very unlikely because we do not observe bond-selective fragmentation. Site-selective fragmentation must be checked at the carbon K edge of this molecule.

Conclusion

Photoelectron–photoion–photoion coincidence mass spectrometry was applied to HMDS Si 2p core ionization. The ion yield spectrum compared to the spectrum of the tetramethylsilane molecule reveals resonances due to the Si–Si chemical bond. The decay is dominated by cascade dissociations of $SiC_3H_9^+$ fragment ion issued from fast dissociation of $HMDS^+$ and $HMDS^{2+}$. Si–Si breaking is the initial step of the fragmentation. The $SiC_3H_9^+$ ion undergoes a statistical decay. Si–C, Si–H, and C–H breaking occur at a later stage. This interpretation is consistent with the loss of memory of the initially excited resonance $(Si–Si)^*$ or $(Si–C)^*$.

Acknowledgment. We thank P. Millie for many helpful comments during this work. T.D. Thomas and T. Baer made enlightening criticisms. We thank H. Bergeron for many helpful

discussions about the rearrangement reactions. R. Thissen helped us during the experimental installation and is gratefully acknowledged.

Appendix: Determination of Calculated Spurious Spectra

If $N^{++}(t_1,t_2)$ represents the number of events during the acquisition time, giving two ions of flight time t_1 and t_2, the occurrence $z(t_1,t_2)$ of this event (t_1,t_2) in the PEPIPICO spectrum is given by

$$z(t_1,t_2) = N^{++}(t_1,t_2)\, f_i(t_1)\, f_i(t_2)\, f_{e2}$$

where $f_i(t_1)$ and $f_i(t_2)$ are the ion detection efficiency at t_1 and t_2 and f_{e2} is the two-electron detection efficiency. The spurious coincidence spectrum is obtained, accounting only for one of two detected ions. At time of flight t we have

$$\mathrm{AC}(t) = \sum_{t_1=0}^{t-1} N^{++}(t_1,t)\, f_i(t)(1-f_i(t_1))f_{e2} + \sum_{t_2=t+1}^{\mathrm{tof}_{max}} N^{++}(t,t_2)\, f_i(t)(1-f_i(t_w))f_{e2}$$

where the increment of 1 in t corresponds to the 1-ns time resolution.

In order to estimate the single/double ionization ratio yield for $SiC_3H_9^+$, we have carried out a very simple probability calculation. If we consider the spurious coincidences corresponding to the $SiC_3H_9^+$ ion, we do not have to take into account the second part of the sum since $SiC_3H_9^+$ is the heaviest detected ion of the spectrum:

$$\mathrm{AC}(t) = \sum_{t_1=0}^{t-1} z(t_1,t)\frac{1-f_i(t_1)}{f_i(t_1)}$$

In the range of the $SiC_3H_9^+$ peak, defined by t_{min} and t_{max}, one obtains

$$\mathrm{AC}(SiMe_3^+) = \sum_{t=t_{min}}^{t=t_{max}} \sum_{t_1=0}^{t_{min}-1} N^{++}(t_1,t)\, f_i(t)(1-f_i(t_1))f_{e2}$$

$$\mathrm{AC}(SiMe_3^+) = N^{++}(SiMe_3^+)\, f_i(SiMe_3^+)(1-\bar{f}_i)f_{e2}$$

where $N^{++}(SiMe_3^+)$ is the total number of $SiC_3H_9^+$ ions formed by the double-ionization process and $\bar{f}_i$ represents the average value of the ion detection efficiency. The simple coincidence spectrum (SIC) contains coincidences due to simple ionization added to the spurious coincidences: $\mathrm{SC}(SiMe_3^+) = \mathrm{AC}(SiMe_3^+) + \mathrm{SIC}(SiMe_3^+)$, with $\mathrm{SIC}(SiMe_3^+) = N^+(SiMe_3^+)f_i(SiMe_3^+)f_{e1}$. $N^+(SiMe_3^+)$ is the total number of $SiC_3H_9^+$ ions formed by the simple ionization process, and f_{e1} is the probability of detecting one electron when only one electron has been ejected.

References and Notes

(1) Nenner, I.; Morin, P.; Simon, M.; Levasseur, N.; Millie, P. *J. Electron Spectrosc. Relat. Phenom.* **1990**, *52*, 623.

(2) Eberhardt, W.; Sham, T.; Carr, R.; Krummacher, S.; Strongin, M.; Weng, S.; Wesner, D. *Phys. Rev. Lett.* **1984**, *50*, 1038.

(3) Lapiano-Smith, D. A.; Ma, C. I.; Wu, K. T.; Hanson, D. M. *J. Chem. Phys.* **1989**, *90*, 2162.

(4) Aksela, H.; Aksela, S.; Mantykennta, A.; Tulkki, J.; Shigemasa, E.; Yagishita, A.; Furusawa, Y. *Phys. Scr.*, to be published.

(5) Ueda, K.; Shigemasa, E.; Sato, Y.; Nagaoka, S.; Koyano, I.; Yagishita, A.; Hayaishi, T. *Chem. Phys. Lett.* **1989**, *154*, 357.

(6) Muller-Dethlefs, K.; Sander, M.; Chewter, L. A.; Schlag, W. *J. Phys. Chem.* **1984**, *88*, 6098.

(7) de Souza, G. G. B.; Morin, P.; Nenner, I. *Phys. Rev. A* **1986**, *34*, 4770.

(8) de Souza, G. G. B.; Morin, P.; Nenner, I. *J. Chem. Phys.* **1989**, *90*, 7071.

(9) Lablanquie, P.; de Souza, A. C. A.; de Souza, G. G. B.; Morin, P.; Nenner, I. *J. Chem. Phys.* **1989**, *90*, 7078.

(10) Litzow, M. R.; Spalding, T. R. In *Mass Spectroscopy of Inorganic and Organometallic Compounds*; Elsevier: Amsterdam, 1973; Chapter 7.

(11) Lappert, M. F.; Padley, J. B.; Simson, F.; Spalding, T. R. *J. Organomet. Chem.* **1971**, *29*, 195.

(12) Flamini, A.; Semprini, E.; Stefani, F.; Sorriso, S.; Gardaci, G. *J. Chem. Soc., Dalton Trans.* **1976**, 731.

(13) Eland, J. H. D. *Laser Chem.* **1991**, *11*, 259.

(14) Simon, M.; Lebrun, T.; Morin, P.; Lavollee, M.; Marechal, J. L. *Nuclear Instr. Meth.* **1991**, *B62*, 167.

(15) Morin, P.; de Souza, G. G. B.; Nenner, I.; Lablanquie, P., unpublished results.

(16) Sette, F.; Stohr, J.; Hitchcock, A. P. *J. Chem. Phys.* **1984**, *81*, 4906.

(17) Szepes, L.; Baer, T. *J. Am. Chem. Soc.* **1984**, *106*, 273.

(18) Berkovitch-Yellin, Z.; Ellis, D. E.; Ratner, M. A. *Chem. Phys.* **1981**, *62*, 21.

(19) Bodeur, S.; Millie, P.; Nenner, I. *Phys. Rev. A* **1990**, *41*, 252.

(20) Forst, W. In *Theory of Unimolecular Reactions*; Academic Press: New York, 1973.

(21) Simon, M.; Lavollee, M.; Lebrun, T.; Delwiche, J.; Hubin, M. J.; Morin, P. *Conf. Proc. Synchrotron Radiation and Dynamic Phenomena*; Beswick, A., Ed.; Grenoble, France, 1991; AIP 258, p 323.

(22) Morin, P.; de Souza, G. G. B.; Nenner, I.; Lablanquie, P. *Phys. Rev. Lett.* **1986**, *56*, 131.

(23) Tamas, J.; Ujszaszy, K.; Szekely, T.; Bujtas, G. *Magyar Kemiai Folyoirat* **1969**, *75*, 148.

(24) Baer, T. *Adv. Chem. Phys.* **1986**, *64*, 111.

(25) Chambers, D. B.; Glockling, F.; Light, J. R. C. *Q. Rev. Chem. Soc.* **1968**, *22*, 317.

(26) De Ridder, J. J.; Dijkstra, G. *Org. Mass Spectrom.* **1968**, *1*, 647.

(27) Gaidis, J. M.; Briggs, P. R.; Shannon, T. W. *J. Phys. Chem.* **1971**, *75*, 974.

(28) Eland, J. H. D. *Acc. Chem. Res.* **1989**, *22*, 281.

(29) Lebrun, T. Ph.D. Thesis, Orsay, France, 1991.

(30) Lavollee, M.; Bergeron, H. *J. Phys. B* **1992**, *25*, 3101.

(31) Eland, J. H. D. *Conf. Proc. Synchrotron Radiation and Dynamic Phenomena*; Beswick, A., Ed.; Grenoble, France, 1991; AIP 258, p 100.